Colloid and Interface Science Communications 66 (2025) 100834

Contents lists available at ScienceDirect

Colloid and Interface Science Communications

journal homepage: www.elsevier.com/locate/colcom

A CFD simulation tool for experimental prediction of inflow polymeric microdroplet formation in a T-junction configuration

Maria Auriemma [a,b,1], Maria Isabella Maremonti [b,1], Edmondo Battista [c], Filippo Causa [b,*]

[a] Center for Advanced Biomaterials for Healthcare@CRIB, Istituto Italiano di Tecnologia (IIT), Largo Barsanti e Matteucci 53, 80125 Naples, Italy
[b] Interdisciplinary Research Centre on Biomaterials (CRIB) and Department of Chemical and Materials Engineering and Industrial Production, University of Naples 'Federico II', Piazzale Tecchio 80, 80125 Naples, Italy
[c] Department of Innovative Technologies in Medicine & Dentistry, University "G. d'Annunzio" Chieti-Pescara, Via dei Vestini, 31, 66100 Chieti, Italy

ARTICLE INFO

Keywords:
Microdroplets
Microfluidics
CFD simulation
Polymeric solutions
T-junction

ABSTRACT

A simulation tool to predict the morphological features and dynamics of polymeric microdroplets in a microfluidic T-junction is presented. A phase-diagram of regimes is created moving from dripping to squeezing within ranges of 10^{-2}–10^{-4} and 10^{-1}–10^{-3} for Reynolds and Capillary numbers, respectively. The simulations show the strong influence of the continuous phase over the droplet size, which changes two orders of magnitude -increasing from 10^{1} to 10^{2} μm- as the flowrate becomes higher.

The phase-diagram allows to choose the optimal fluid-flow conditions to have a precise and stable dripping production of spherical drops. Indeed, a successful down-scaling of drop size up to ~10^{1} μm with a drop rate production of ~40 drops/s is obtained, with a great accordance between simulative and experimental results (error < 1 %), at high monodispersity (polydispersity index<0.05). Therefore, our tool has proved to be a powerful approach to predict and regulate polymeric microdroplet production in microfluidics.

1. Introduction

In recent years, polymeric spherical microdroplets gained a lot of attention in several fields especially for biological and chemical applications. In general, the interest to produce polymeric microdroplets is due to their appreciable properties of biocompatibility, biodegradability with tuneable rheological and mechanical properties [1,2]. Indeed, the use of polymeric droplets -in a size range of 10 to 10^{2} μm- extends from microreactors for catalysis and chemical synthesis, point-of-care diagnostics, drug delivery, cell/molecule compartmentalization and diagnostic testing [2–4]. Depending on the specific application, microdroplets needs to be of different sizes and passing through a downsize -from hundreds to few microns in diameter- becomes crucial [5]. However, a precise control of size, shape and monodispersity of polymer microdroplets is still challenging because of the high viscosity and interfacial tensions in liquid-liquid contact conditions. Moreover, classical techniques to produce microdroplets -such as atomization, emulsion, suspension polymerization or high-speed stirring- are affected by high polydispersity, low throughput and not tuneable sizes and shapes [6].

Microfluidic-based approaches become necessary to create efficient tools for a controlled production of microdroplets [7,8]. In detail, microfluidic platforms provide a great control over the size and shape and offers the capability to manipulate few volumes of fluids. Droplets are obtained starting from two immiscible liquids -continuous (c) and dispersed (d) phases- with specific material properties. Depending on the device geometry, different configurations of crossflow, co-flow and flow-focusing can be used for droplet production [9]. For example, crossflow is characterized by a T-junction configuration where c- and d-phases can be manipulated to obtain different flow regimes -like dripping and squeezing- leading to the formation of droplets of variable sizes and shape. The dripping occurs when shear forces dominate over the interfacial forces between the two fluids, creating individual spherical droplets. Instead, the squeezing regime provides droplets/slug objects that adhere to the channel walls [10,11]. Therefore, by changing the flowrates of c- and d- phases and tuning their viscosity and interfacial tension properties, it is possible to modulate size, shape, dispersity and regime of droplet formation [12].

To predict droplet generation, multiphase and volume of fluids (VOF) models are often used in computational fluid dynamics (CFD)

* Corresponding author.
E-mail address: causa@unina.it (F. Causa).
[1] These authors contributed equally.

https://doi.org/10.1016/j.colcom.2025.100834
Received 23 October 2024; Received in revised form 22 March 2025; Accepted 23 March 2025
Available online 3 April 2025

numerical simulations, investigating and optimizing the best fluid-dynamic conditions for droplet formation [10,13–16], reducing the experimental costs. In detail, VOF simulations of liquid-liquid flows in microchannels, demonstrated to be useful for prediction and simulation of droplet generation in different flow regimes, playing with device geometry as well as with imposed fluid-flow conditions [15–19].

In T-junction geometry, most of works in literature focus on water-in-oil microdroplets formation [20–25]. Indeed, the use of polymeric solutions has been less studied since the intrinsic shear-dependent properties of the fluid make difficult the precise characterization of the droplet breakup dynamics and of the resulting size monodispersity [26]. Moreover, even if considerable research works have been devoted to experimentally reveal the breakup mechanisms of low-viscosity polymeric solutions [17,27], none of these provide a controlled and optimized process of microdroplet production.

For these reasons, it is important to provide a simulation solution to predict the efficacy of a commercial T-junction microfluidic geometry in producing polymeric microdroplets in a wide range of sizes and shapes passing through the optimization of desired regime for obtaining spherical drops, minimizing their size and guaranteeing a high monodispersity of the population, without paying in time-consuming experimental procedures or elevated computational costs for simulations.

Here, a two-dimensional (2D) simulation tool is presented to predict the fluid-dynamic conditions to produce different sized and shaped polymeric microdroplets inside a T-junction geometry, to obtain a precise, tuneable and scalable process. For two different liquid-liquid interfaces -where the dispersed is a polymeric solution at different concentration and the continuous is an oil- we demonstrated that polymeric microdroplets change both in size and shape in a wide-range of applied flowrates, spacing from dripping to squeezing regime. The implementation of a 2D CFD simulation allowed for the prediction of microdroplet size, shape and inflow dynamics. From this, a phase

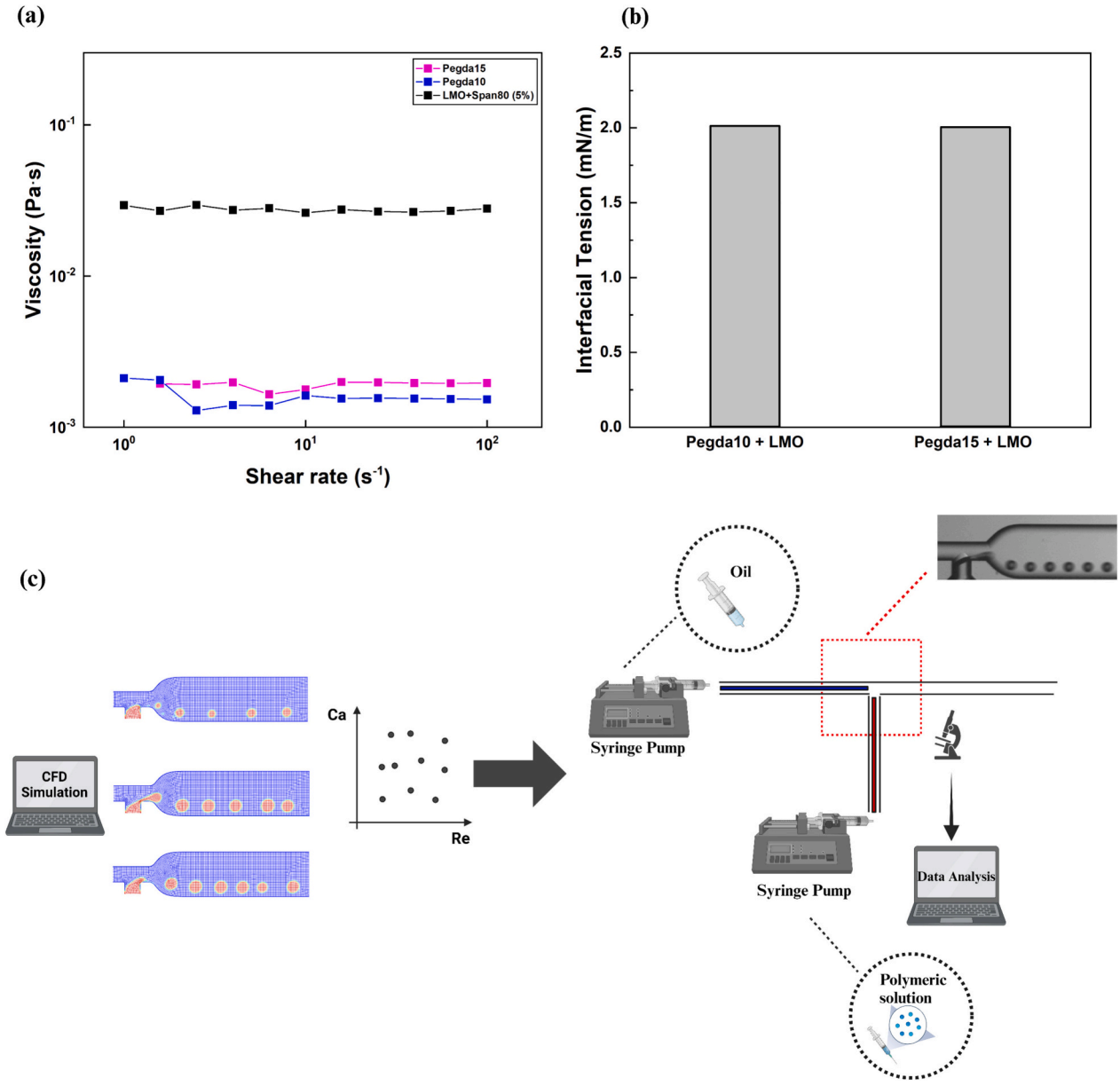

Fig. 1. (a) Flow curve viscosity for Pegda10, Pegda15 and LMO + Span80. All the fluids exhibit a Newtonian behaviour. (b) interfacial tension between Pegda10-LMO, and Pegda15-LMO. (c) After the collection of simulative results, the experiments were performed. Two syringe pumps were used to inject c- and d-phases. The droplets were observed in flow through a live microscope and a droplet monitor software; then they were collected in a collection chamber. The inset is an inflow droplet production record.

diagram of regimes was obtained, precisely defining a map of non-dimensional parameters ranges where the different production regimes are defined. In detail, we found that dripping occurs ranging Reynolds (Re) and Capillary (Ca) numbers of the continuous phase from 10^{-3} to 10^{-2} and, in that range, further experimental validations were provided, demonstrating a reliable scaling-down of the final drop diameter. A great accordance with the simulative data was obtained (relative error < 1 %) and a minimum drop size of ~40 μm was produced.

The presented approach predicts and controls polymeric micro-droplets formation in T-junction geometry, giving the opportunity to precisely tune the fluid dynamic conditions and fluid rheological and interfacial properties, necessary to obtain the desired shape and size for the prescribed aim of use the produced drops.

2. Materials and methods

2.1. Materials

The used liquids were characterized in terms of viscosities and interfacial tension between c- and d-phases (Fig. 1). The viscosities were measured by a stress-controlled double Couette rheometer (MCR 302, ANTON PAAR). In detail, light mineral oil (LMO, M6904, 8042-47-5 from Sigma-Aldrich) with 5 % (*v*/v) SPAN 80 (S6760, 1338-43-8, from Sigma-Aldrich) as surfactant agent were used as c-phase. Instead, two Polyethylene glycol diacrylate (Pegda700, 455,008, 26,570–48-9, from Sigma-Aldrich) solutions at 10 % (*w/v*) and 15 % (w/v) concentration, named Pegda10 e Pegda15, were chosen as d- phase (Fig. 1). The working shear rate do not lead to shear-thinning behaviours of the Pegda solutions. The interfacial tension between c- and d-phases was measured using the pendant drop method with Attension by KSV instruments tensiometer and the correspondent Attension Theta Software. Moreover, we defined a viscosity ratio between the two phases as $\lambda = \eta_d/\eta_c$.All the values of the mentioned parameters are reported in Table S1.

2.2. Mathematical model and numerical simulation

The numerical model was realized by employing the CFD package Ansys Fluent®, Academic version 2023, on a processor 13th Gen Intel® Core ™ i9-13900K, 3 GHz and 32 GB of RAM.

All numerical simulations were performed using a 2D computational space. The advantages of 2D simulation consist of there are no input flowrate along the depth direction and the third dimension of momentum conservation equations can be neglected. Moreover, there is a strong reduction in computational costs, and the 2D computation results to be highly reproducible [17,27].

We used the VOF method to reproduce the dynamics of droplet formation of Pegda10-Pegda15 in light mineral oil and span 80 at 5 %. The liquids are considered incompressible, immiscible, Newtonian, and characterized by constant material properties. For the multiphase model, it was necessary to introduce a new variable, α, representing the volume fraction of each phase. Defining α_q -q^{th} fluid's volume fraction in the grid cell- there are three possible conditions: $\alpha_q = 0$, the cell does not contain the q^{th} fluid. $\alpha_q = 1$, the cell contains only the q^{th} fluid. $0 < \alpha_q < 1$, the cell contains the interface between the q^{th} fluid and one or more other fluids [14].

The used model is a two-phase system. The indexes 1 and 2 stand for phase 1 and phase 2, respectively. Then, density and viscosity are expressed as [28]:

$$\rho = \alpha_2\rho_2 + (1-\alpha_2)\rho_1$$

$$\eta = \alpha_2\eta_2 + (1-\alpha_2)\eta_1$$

Therefore, in VOF, the momentum equation is written as:

$$\frac{\partial(\rho U)}{\partial t} + \nabla \bullet (\rho U \bullet U) = -\nabla P + \nabla \bullet \left[\eta\left(\nabla U + \nabla U^{T}\right)\right] + (\rho g) + F$$

And the continuity equation as:

$$\frac{\partial(\rho)}{\partial t} + \nabla \bullet (\rho U) = \sum_q S_q$$

Where *ρ, U, t, S, η* are density, velocity, time, mass source and viscosity, respectively. Here, the term S is zero.

The interfacial tension between the two fluids is expressed as [29].

$$F = \gamma\left[\frac{\rho k\hat{n}}{\left(\frac{1}{2}\right)(\rho_1+\rho_2)}\right]$$

k=$\nabla \bullet \hat{n}$;

$\hat{n} = n/|n|$ and n=$\nabla \bullet \alpha_q$.

Where γ is the interfacial tension, $\hat{n}$ the normal versor and *k* the local curvature [29]. The solver works through spatial and time variations. Mainly, the spatial derivatives were discretized by using the QUICK scheme, and a first order implicit derivatives were used for time discretization. For the pressure-velocity coupling, we adopted the COUPLED algorithm, and the gradients were calculated by Green-Gauss cell-based method. An initial time step size of 10^{-5} and 6000 time steps were used for numerical stability. The adaptive mesh refinement method was selected to refine the continuous-dispersed phases interface [13]. The contact angle was specified as a measure of the wall repulsion towards the fluid flows. It was fixed at 160°, for all simulations. Concerning the boundary conditions, the two liquid inlets were designed as velocity inlets, the outlet as pressure-outlet. Moreover, the no-slip condition to the channel walls was applied. The fluid-flow analysis was based on a set of non-dimensional numbers [30]. Reynolds number is used to tune and control the inertial and viscous forces, expressed as:

$$Re = \frac{\rho v d_h}{\eta}$$

It was fixed $Re << 1$, for a Stokes regime.

Where *ρ, v, η* are the density, average velocity and viscosity of the fluid phase, respectively.

d_h is the hydraulic diameter of the channel,

$$d_h = \frac{2wh}{w+h}$$

With *w* and *h* as the channel width and the depth, respectively.

The Capillary number, defined as the ratio between viscous and interfacial forces,

$$Ca = \frac{\eta v}{\gamma}$$

Moreover, to better control the process, it was important to calibrate not only the single flowrate of the phases but also the ratio between them (*ϕ*),

$$\phi = \frac{Q_d}{Q_c}$$

To verify the predicted fluid-dynamic conditions, an experimental setup was used (Fig. 1).

We purchased a T-junction glass chip (Dolomite Microfluidics, cod. 3,000,158), in which the two phases were pushed into the respective channels through a syringe pump (Nemesys-Low pressure NEM-B101–02 E) to provide stable and reproducible flow. Videos of droplets were acquired using a droplet monitor software.

3. Device geometry and mesh convergence study

The T-junction geometry with relative dimensions is reported in Fig. 2. The original geometry, based on Dolomite Microfluidics system, consists of two inlets -one for the c-phase and one for d-phase- and outlet through which the droplets pass. The channel width is 300 μm, while the h is 100 μm along the entire channel. For the simulation, the device geometry was optimized, to reduce the computational costs. Moreover, imposing the Cauchy continuity principle, we fixed the fluid velocity magnitude at the two inlets (Fig. 2a-b).

For the best optimization of the simulation, a mesh convergence study was necessary. Firstly, two set of three mesh element size were selected, defining fine (L = 1 μm; 1.5 μm; 2.25 μm) and coarse (L = 3 μm; 5 μm;7 μm) grids, each one characterized by a certain number of nodes and cells (Table 1). Defining the grid refinement ratio as [31]:

$$r = \frac{L_{COARSE}}{L_{FINE}}$$

in this work r is 1.4–1.5, according to literature findings [32].

To establish the quality of the mesh convergence study, we decided to compare the experimental results of a T-junction configuration already used by the group with a certain couple of flowrates for which a stable dripping occurs producing droplets in a dimensional range of 72.6 and 77.4 μm ($Q_d = 0.25\ \mu L/min$ - $Q_c = 2.5\ \mu L/min$, with $\phi = 0.1$- where d and c stand for d- and c- phase flowrates)

[33].

The relative percentage errors between two adjacent mesh element size were computed as [31]:

$$\varepsilon = \frac{x_{fine} - x_{coarse}}{x_{fine}}$$

Where x is the produced droplet diameter (D_{drop}) and the velocity magnitude (Fig. 2c-d). The velocity profile was calculated along a reference cut line (Fig. 2b), chosen according to the region where the velocity profile changes significantly. The coarse set of mesh element sizes provides the smallest errors. In details, we decided to use the 7 μm mesh size, which returns a $D_{drop} = 80.62 \pm 0.34\ \mu m$, with $\varepsilon < 10\%$. Moreover, for the chosen mesh, aspect ratio and skewness are 1.35±0.93 and 0.03±0.07, respectively.

Table 1
Mesh element size used in mesh independence test. Two triad of mesh sizes (fine and coarse) are reported.

	Mesh size (μm)	N_{nodes}	N_{cells}
Fine	1	349,369	347,803
	1.5	156,748	155,699
	2.25	70,792	70,085
Coarse	3	29,856	29,405
	5	15,073	14,750
	7	8085	7845

4. Results and discussion

In this section, we present relevant results -both simulative and experimental- to validate the efficient prediction of regime production for polymer microdroplets of different sizes and shapes in a T-junction geometry.

4.1. Simulative optimization of T-junction geometry

To establish the best conditions which lead to a stable droplet formation in a wide range of monodispersed diameters, we characterized different fluid dynamic regimes for the T-junction geometry.

Using $\phi = 0.1$ as starting value, we explored the influence of Q_c on

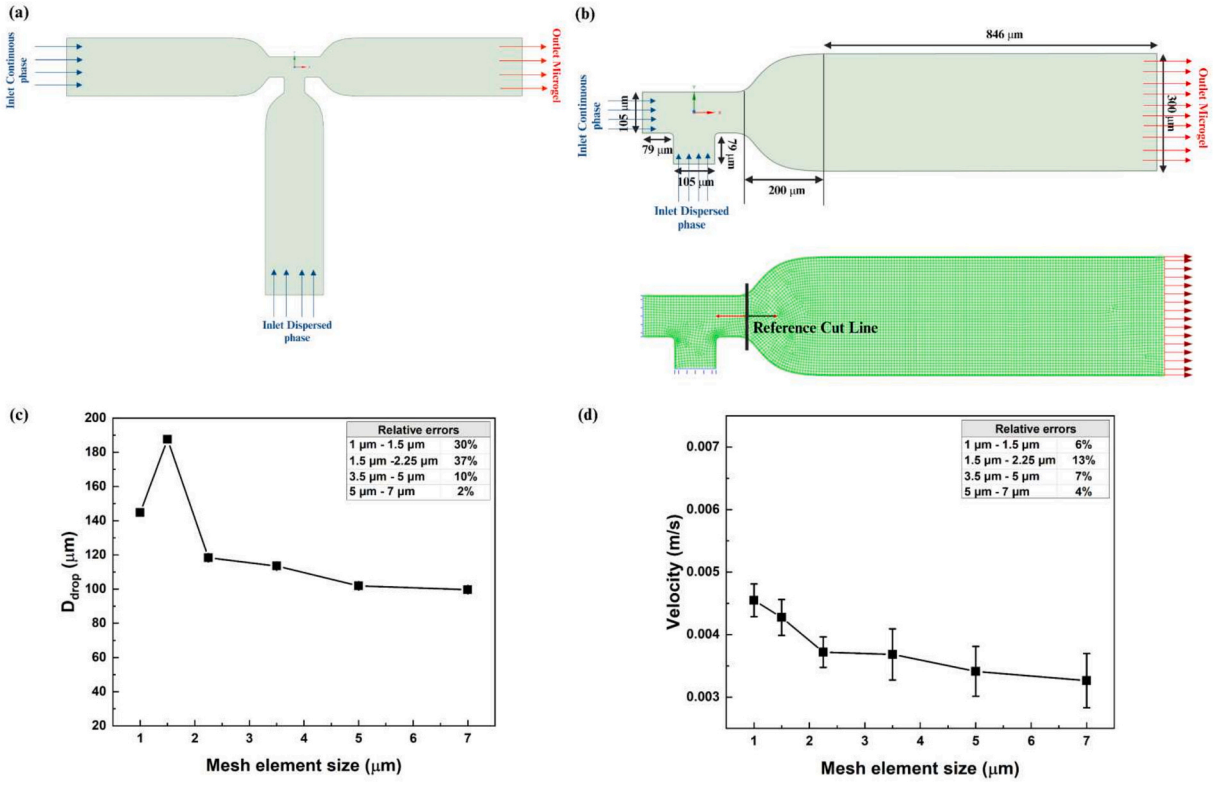

Fig. 2. T-junction geometry domain and mesh convergence study. (a) Complete geometry design that reproduces Dolomite Microfluidics device. (b) Geometry design simplification used for the implementation of CFD simulations, with relative dimensions. On the bottom, schematic representation of the reference cut line, along which the velocity profile was calculated, as regard as the mesh independence test. (c) D_{drop} *vs* mesh size. (d) Average velocity *vs* mesh size, along the reference cut line. The insets show the relative percentage errors between two adjacent mesh size.

droplet formation, for two different values of Q_d (0.25 and 0.5 μl/min). In detail, we analysed the influence of the resulting ϕ on microdroplet formation, exploring both changes in size and shape. In general, for a pure water-in-oil microemulsion formation in T-junction, it has been shown that the droplet size -intended as the major diameter of a slug-like shape- increases when the Q_c decreases [20,34].

Therefore, here we report the variation of the droplet/slug mean diameter D_h with respect to ϕ, where $D_h = 4S/l$, with S and l being the area and the perimeter of the slug, respectively. The need to define droplet/slug dimension with D_h is that there is not only a variation in dimension but also in the shape of the produced objects, under the variation of Q_c and Q_d (Fig. 3). Indeed, the different values of ϕ revealed

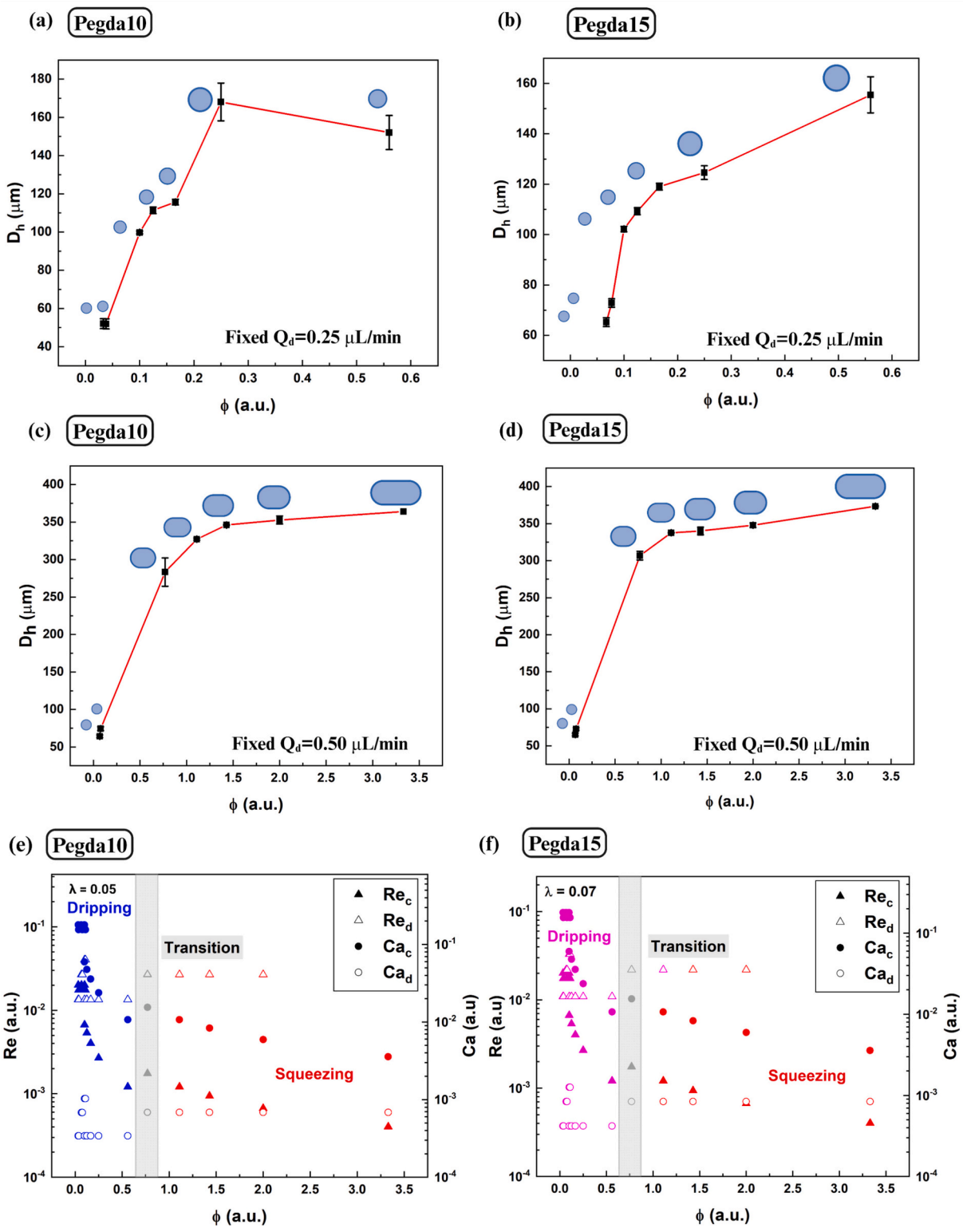

Fig. 3. Microdroplet shape variation and production regime depending on non-dimensional parameters. (a) and (c) D_h of spherical droplets is plotted against ϕ, for Pegda10 at fixed Q_d. (b) and (d) D_h of spherical-slug droplets is plotted against ϕ, for Pegda15 at fixed Q_d. (e) and (f) *Re* and *Ca* numbers of c- and d-phases are plotted against ϕ -for Pegda10 and Pegda15- and three possible regimes are defined (dripping-transition-squeezing), at $\lambda = 0.05$ and $\lambda = 0.07$.

that this ratio affects the flow regimes, the size and shape of the produced droplets. Increasing ϕ, droplet diameters increase. At fixed Q_d= 0.25 μL/min, it is possible to note that the last two points show a slight decrease in diameter when $\phi \sim 0.6$ (Fig. 3a, Supplementary Material Fig. S1). This is possibly due to a simulation instability where also satellite drops start to appear. Instead, Pegda15 has a more stable behaviour, even increasing ϕ. The discrepancy between Pegda10 and Pegda15 is due to the difference in η, which is higher for Pegda15. Viscous contribution becomes even more relevant in drop formation, leading to more stable dripping without relative fluid-flow instabilities.

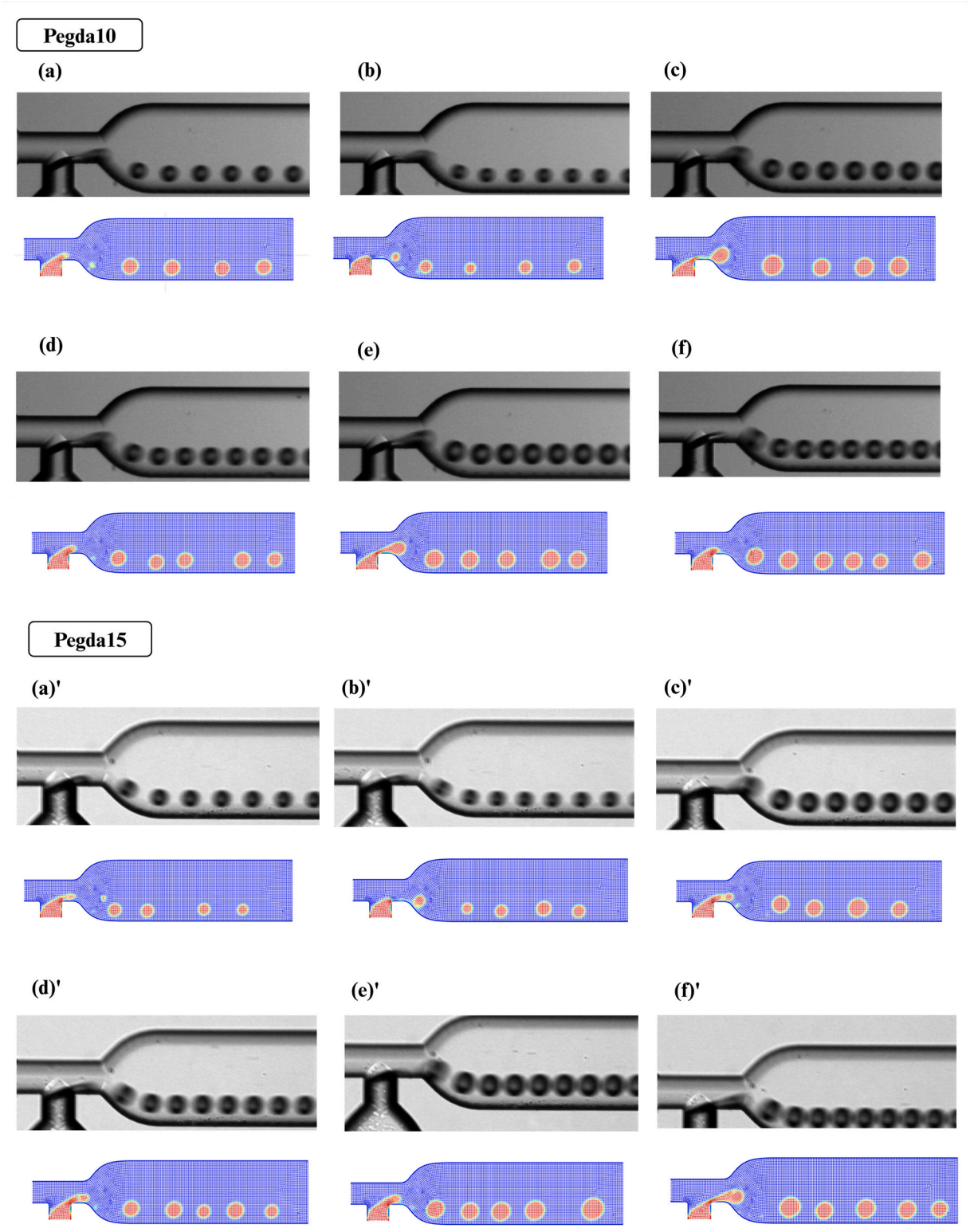

Fig. 4. Comparison between simulation and experiment for Pegda10 and Pegda15. Schematic representation of six fluid-dynamic conditions, as simulation-experiment comparison: a-a') Q_d=0.25 μL/min - Q_c=6.5 μL/min; b-b') Q_d=0.25 μL/min - Q_c=7.5 μL/min; c-c') Q_d=0.5 μL/min - Q_c=6.5 μL/min; d-d') Q_d=0.5 μL/min - Q_c=7.5 μL/min; e-e') Q_d=0.75 μL/min - Q_c=6.5 μL/min; f-f') Q_d=0.75 μL/min - Q_c=7.5 μL/min.

At fixed Q_d=0.5 μL/min, at high value of ϕ (Fig. 3b and d, Supplementary Material Fig. S1) lowering the c-phase flowrate, the squeezing becomes dominant on the dripping regime. Instead, for both 0.25 and 0.5 μL/min conditions, slight changes in Q_c lead to a stable dripping regime, even in a small range ϕ, where it is possible to scale down the microdroplets diameter up to ~40 μm.

Addressed the importance of the ϕ variation in microdroplet formation, we decided to further extend the flowrate dataset to create a map of different fluid dynamic conditions to predict both sizes and shapes of microdroplets. By varying *Re*, *Ca* and ϕ numbers a flow regime-diagram is presented (Fig. 3e-f). For T-junction, increasing *Ca* of the c-phase, the transition from squeezing to dripping is expected. $Ca \sim 10^{-2}$ indicates the transition value from one regime to another [35].

Indeed, with our system, it comes out that dripping regime occurs -at low ϕ- with a $10^{-2} < Re < 10^{-1}$ and $10^{-3} < Ca < 10^{-1}$, for c- and d-phases of both Pegda10 or Pegda15. From dripping to squeezing, it was highlighted a transition region, which occurs at $0.6 < \phi < 0.8$. This transition is obtained as the c-phase *Re* and *Ca* decrease, without a relevant contribution from the d-phase fluid flow. Moreover, as the dripping approaches to become squeezing, a power-law like distribution of the scatter points is shown. Such a trend of variation goes in accordance with the scaling of drop sizes typically measured in T-junction configurations with water-oil interfaces [21,36,37].

4.2. Experimental inflow drop formation

From the regime-diagram, we selected a set of dripping conditions to produce spherical polymeric microdroplets. In detail, our aim was to demonstrate the powerful prediction obtained from the simulations in scaling-down the size of the drops. From the map, ranging *Re* and *Ca*, we were able to reduce the microdroplet size even in a small range of ϕ. In details, we moved in the map of the regimes with $Re \sim 10^{-2}$ and $Ca \sim 10^{-1}$ to obtain a stable dripping for spherical drops. Instead, ϕ scales from 10^{-2} to 10^{-1}.

The chosen couples of flowrates are reported in Table S2. As a result, the simulation provided a great prediction of the droplet pinch-off and dynamics (Fig. 4; video 1-video 12 in Supplementary material).

To quantitively compare the experimental and simulative results, we measured the D_{drop} and the droplet distances from the wall ($H_{drop-wall}$) for both Pegda10 and Pegda15 (Supplementary Material Fig. S2). Moreover, a percentage relative error was calculated to estimate the agreement between the results. It was computed as [38],

$$\varepsilon_{\%} = \frac{\left|\overline{x}_{exp} - \overline{x}_{sim}\right|}{\overline{x}_{exp}} \bullet 100$$

Where $\overline{x}_{exp}$ and $\overline{x}_{sim}$ are the experimental and simulation results, respectively. In detail, D_{drop} and $H_{drop-wall}$ were measured through ImageJ. For both parameters, the lowest errors are for the first two couple of flowrates with $\varepsilon_{\%} \sim 1\%$ (Supplementary Material Fig. S2).

A lower Q_d guarantees a greater stability of the fluid-dynamic condition as well as a strong reduction of the size. Indeed, the simulated inflow dynamics of microdroplets replicates the one observed experimentally (Supplementary material Fig. S2). Moreover, ϕ-variation strongly influences the pinch-off dynamics of droplets. This agrees with the regime changes reported in the map, since increasing ϕ the fluid dynamics passes through the transition towards the squeezing region (Fig. 4). Of note, Pegda15 tends to elongate more the pinch-off region when the Q_d increases. In addition, as expected during the neck rupture stage at higher viscosity ($\lambda = 0.07$) [26], the width of droplet neck decreased, and the size of satellite droplet increased -optimizing monodispersity (Supplementary Material Table S3 and S4)- as the fluid velocity increases as well.

To further establish the precision of the obtained data, we reported monodispersity of the obtained droplet populations, as quality indicator of the microdroplet production both in simulation and experimental conditions (Supplementary Material Table S3 and S4). Dispersity data are of great importance to have an idea of the produced emulsion stability. In general, macroemulsion with final sizes between 1 and 100 μm suffer from elevated polydispersity index (>0.4) which could often translate into instability phenomena (*e.g.* over time, phase separation could occur) [39].

Therefore, obtaining a polydispersity index less than 0.05 in all the explored conditions confirm a high stable production process (Supplementary Material Table S3 and S4).

Therefore, to demonstrate the robustness of the presented predictive tool for polymeric microdroplet production in T-junction configuration, we decided to report the normalized values of the mean diameters ($D^* = \frac{\overline{D}}{\overline{D}_{max}}$) and of the distances ($H^*_{drop-wall} = \frac{\overline{H}_{drop-wall}}{\overline{H}_{drop-wall,max}}$). Such normalized values of the obtained data allow us to define trends curves, as scaling laws specific for certain fluid dynamics conditions.

As a function of ϕ, we reported the variation of D^* and $H^*_{drop-wall}$ for both Pegda10 and Pegda15 (Fig. 5). Except for Pegda15 where both the normalized values scale in the same way with respect to the ϕ in simulation and experiments, Pegda10 shows some differences both as slope and trend in the $H^*_{drop-wall}$. Such discrepancy is attributed to the way in which the dispersed phase interacts with the continuous one is different, since λ-values change between Pegda10 and Pegda15. Indeed, a more pronounced neck is visible at the junction, which can be translated in a different droplet's dynamics not only as formation but also as inflow motion. Therefore, in our polymeric microdroplet production, we verified that the competition between viscous and inertial forces result to be less relevant than the nominal effect of the applied flowrates and the interfacial forces between the two phases. Other relevant parameters for the evaluation of the T-junction performance are related to the drop velocity ($\sim \frac{displacement}{time}$) and frequency of production [21,40]. In our experiments and simulation, drop velocity ranges from 1.5 to 2.5 mm/s with a $\varepsilon_{\%} < 20\%$ for both Pegda10 and Pegda15 (Supplementary Material Table S5 and S6). As rate of production, it is known that such a frequency term is highly dependent on imposed fluid flow conditions. In particular, we used the formulation of production rate as follows [40,41]:

$$production\ rate = \frac{drop\ velocity}{spacing\ drops}$$

Where such a spacing indicates the distance between two consecutive drops centre. For Pegda10 and Pegda15, we estimated a mean frequency of production of ~25 drops/s and ~ 30 drops/s (Supplementary Material Table S5 and S6). Such a difference between the two is deputed to the spacing of the droplets which is higher for Pegda15 but compensated by the lower velocity since more viscous than Pegda10.

As a result, using the regime-diagram for the preferred fluid dynamics and then the scaling factor of the desired size, we demonstrate the possibility to precisely define the best production condition.

5. Conclusion

In the current study, we presented a simulation tool for the prediction and control of microdroplet formation in a T-junction microfluidic configuration. Thanks to a large set of two dimensional CFD simulations, we were able to define a phase diagram of possible fluid-dynamic regimes useful to produce polymeric microdroplets. By variation of *Re* and *Ca* numbers as a function of ϕ, it was possible to read the corresponding droplet formation regime and the expected resulting size. We identified a transition between dripping to squeezing regimes in a T-junction geometry, then optimizing both the size and the shape of the droplets. With the aim to produce spherical droplets with a dimension less than 10^2 μm, we decided to implement a set of simulations and experimental tests working in a dripping regime, far enough from the transition, minimizing the size.

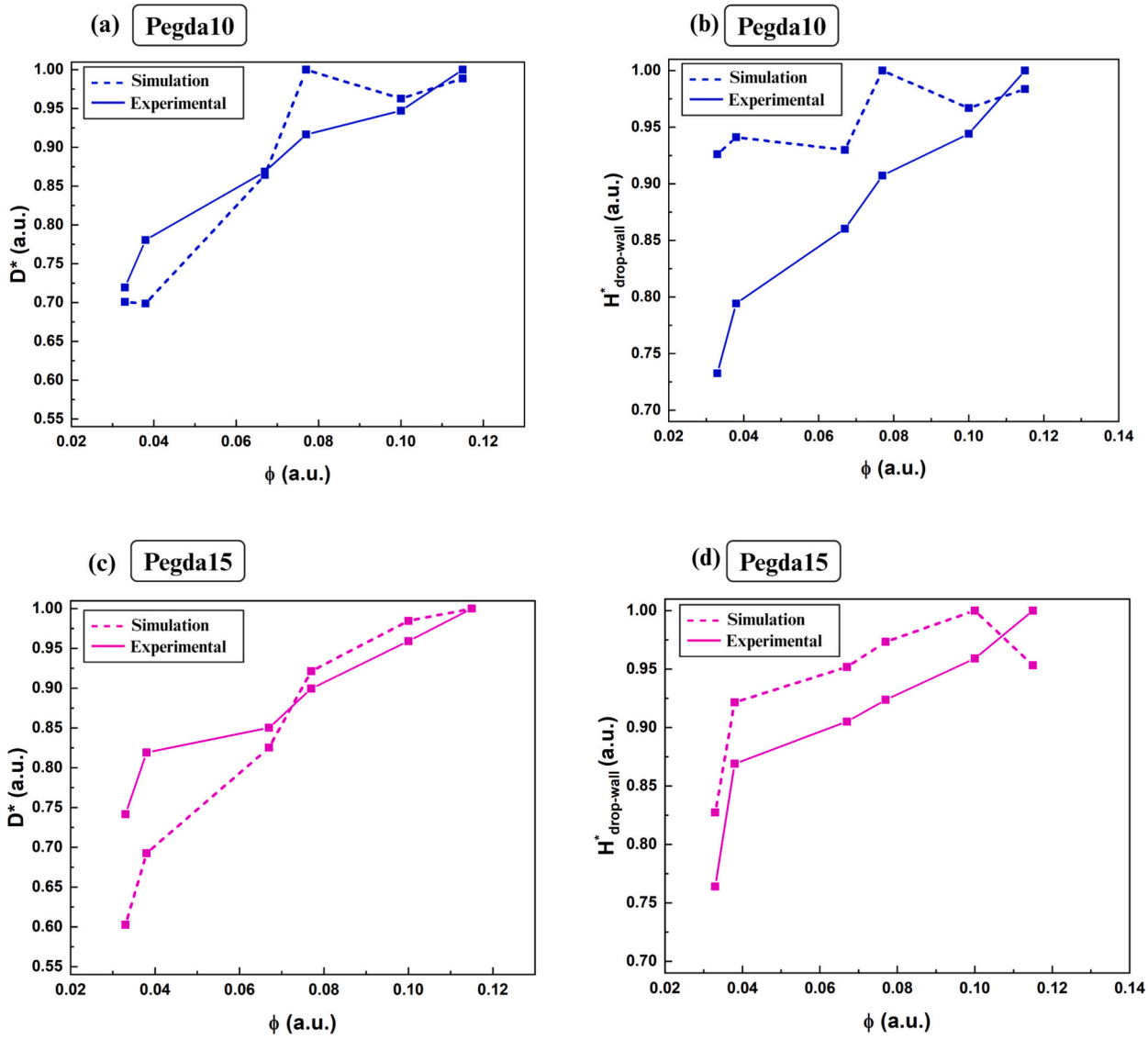

Fig. 5. Normalized droplets mean diameter (D^*) and distances from the wall ($H^*_{drop-wall}$), as a function of ϕ, for Pegda10 (a-b) and Pegda15 (c-d).

Main achievements of the research work are here reported:

- precise prediction and control of the fluid dynamic conditions for a T-junction geometry have been provided for the formation of spherical droplets in a dripping regime;
- for a very small range of ϕ -from 0.03 to 0.1- we were able to finely tune the microdroplet production with a wide-range of droplet sizes (10^1–10^2 μm);
- high monodispersity of droplet populations was obtained (polydispersity index <0.05);
- thanks to the tight control of the fluid flows, a minimum size of ~40μm was reached -even if the T-junction section is of hundreds of μm- with a relative error of 1 % with respect to simulative results.

We are conscious that the choice to work in a two-dimensional field strongly influences both the formation and the inflow dynamics of the droplets. However, since the relative errors remain less than 20 % in all the presented cases, the reduction of the computational costs and the easy way to implement the simulations result to be powerful for the creation of the presented tool. Indeed, both the flow regime diagram and the trend plots of the expected diameters are easy-to-use instruments to approach to a droplet formation problem in a T-junction like configuration.

In conclusion, we believe that our study could provide guidelines to manage polymer fluids to create microdroplets in a controlled manner with a reduced size in a T-junction geometry, for the final creation of functionalized particles useful for those interested in biological, food and chemistry applications. As a future perspective, the simulative prediction could become a real-time process to completely automate the microfluidic system, eventually providing a feedback control loop for the rearrangement of the flow rates to produce the drops of desired size and shape directly online into the microfluidic device. Moreover, the simulation tool remains highly versatile and useful also for the characterization of other production regimes with other liquid-liquid interfaces.

Supplementary data to this article can be found online at https://doi.org/10.1016/j.colcom.2025.100834.

CRediT authorship contribution statement

Maria Auriemma: Writing – review & editing, Writing – original draft, Validation, Methodology, Investigation, Formal analysis. **Maria Isabella Maremonti:** Writing – review & editing, Writing – original draft, Validation, Methodology, Investigation, Data curation. **Edmondo**

Battista: Writing – review & editing, Investigation. **Filippo Causa:** Writing – review & editing, Supervision, Project administration, Funding acquisition, Conceptualization.

Declaration of competing interest

The authors declare the following financial interests/personal relationships which may be considered as potential competing interests:

Filippo Causa reports financial support was provided by Italian Ministry of University and Research. If there are other authors, they declare that they have no known competing financial interests or personal relationships that could have appeared to influence the work reported in this paper.

Acknowledgements

The authors acknowledge the support by the Italian Ministry of University and Research (National recovery and resilience plan funding): "National Centre for Gene Therapy and Drugs based on RNA Technology", CUP: E63C22000940007, CN3 Task3.

Data availability

Data will be made available on request.

References

[1] R. Samanipour, Z. Wang, A. Ahmadi, K. Kim, Experimental and computational study of microfluidic flow-focusing generation of gelatin methacrylate hydrogel droplets, J. Appl. Polym. Sci. (2016) 133.
[2] E.Y. Basova, F. Foret, Droplet microfluidics in (bio)chemical analysis, Analyst 140 (2015) 22–38.
[3] H. Shi, K. Nie, B. Dong, M. Long, H. Xu, Z. Liu, Recent Progress of microfluidic reactors for biomedical applications, Chem. Eng. J. 361 (2019) 635–650.
[4] E. Battista, S. Napoletano, M.I. Maremonti, D. Dannhauser, P.A. Netti, F. Causa, Scopusresults, in: Proceedings of the Microgels as a Biosensing Platform, Patron Editore S.r.l, 2023.
[5] M.P. Stewart, R. Langer, K.F. Jensen, Intracellular delivery by membrane disruption: mechanisms, strategies, and concepts, Chem. Rev. 118 (2018) 7409–7531.
[6] A. Gaillard, R. Sijs, D. Bonn, What determines the drop size in sprays of polymer solutions? J. Nonnewton. Fluid Mech. 305 (2022) 104813.
[7] L. Amirifar, M. Besanjideh, R. Nasiri, A. Shamloo, F. Nasrollahi, N.R. De Barros, E. Davoodi, A. Erdem, M. Mahmoodi, V. Hosseini, et al., Droplet-based microfluidics in biomedical applications, Biofabrication (2022) 14.
[8] T. Moragues, D. Arguijo, T. Beneyton, C. Modavi, K. Simutis, A.R. Abate, J.C. Baret, A.J. deMello, D. Densmore, A.D. Griffiths, Droplet-based microfluidics, Nat. Rev. Methods Prim. (2023) 3.
[9] Y. Liu, Y. Li, A. Hensel, J.J. Brandner, K. Zhang, X. Du, Y. Yang, A review on emulsification via microfluidic processes, Front. Chem. Sci. Eng. 14 (2020) 350–364.
[10] M. Rahimi, A. Shams Khorrami, P. Rezai, Effect of device geometry on droplet size in co-axial flow-focusing microfluidic droplet generation devices, Colloids Surf. A Physicochem. Eng. Asp. 570 (2019) 510–517.
[11] N.M. Kovalchuk, M. Sagisaka, K. Steponavicius, D. Vigolo, M.J.H. Simmons, Drop formation in microfluidic cross-junction: jetting to dripping to jetting transition, Microfluid. Nanofluid. (2019) 23.
[12] P. Zhu, L. Wang, Passive and active droplet generation with microfluidics: a review, Lab Chip 17 (2017) 34–75.
[13] I.L. Chaves, L.C. Duarte, W.K.T. Coltro, D.A. Santos, Droplet length and generation rate investigation inside microfluidic devices by means of CFD simulations and experiments, Chem. Eng. Res. Des. 161 (2020) 260–270.
[14] A.B. Desamala, A.K. Dasmahapatra, T.K. Mandal, Oil-water two-phase flow characteristics in horizontal pipeline-a comprehensive CFD study, in: World Academy of Science, Engineering and Technology international journal of chemical, molecular, nuclear, materials and metallurgical Engineering Vol:8, No:4, 2014.
[15] R. Raj, N. Mathur, V.V. Buwa, Numerical simulations of liquid-liquid flows in microchannels, in: Proceedings of the Industrial and Engineering Chemistry Research Vol. 49, 2010, pp. 10606–10614.
[16] Y. Amini, V. Ghazanfari, M. Heydari, M.M. Shadman, A.G. Khamseh, M.H. Khani, A. Hassanvand, Computational fluid dynamics simulation of two-phase flow patterns in a serpentine microfluidic device, Sci. Rep. (2023) 13.
[17] M. Soroor, M. Zabetian Targhi, S.A. Tabatabaei, Numerical and experimental investigation of a flow focusing droplet-based microfluidic device, Eur. J. Mechan. B/Fluids 89 (2021) 289–300.
[18] X. Li, L. He, Y. He, H. Gu, M. Liu, Numerical study of droplet formation in the ordinary and modified T-junctions, Phys. Fluids 31 (2019).
[19] K.V. Rodríguez Granado, S.L. Anna, L.R. Rojas-Solórzano, S. Verma, Numerical simulation of droplet formation in a microchannel device, Intern. J. Multiphys. 7 (4) (2013) 271–286.
[20] N.T. Thai, C.T. Xuan, P.D. Thanh, M.A. Tuan, N.P. Nhung, Formation of microdroplet in T-junction microfluidic system: experiment and simulation, Commun. Phys. 28 (2018) 225.
[21] S.K. Jena, S.S. Bahga, S. Kondaraju, Prediction of droplet sizes in a T-junction microchannel: effect of dispersed phase inertial forces, Phys. Fluids 33 (2021).
[22] H. Liu, Y. Zhang, Droplet formation in a T-shaped microfluidic junction, J. Appl. Phys. 106 (2009).
[23] Z. Liu, J. Zhao, Y. Pang, X. Wang, Generation of droplets in the T-junction with a constriction microchannel, Microfluid. Nanofluid. (2018) 22.
[24] D. Pan, Y. Zhang, T. Zhang, B. Li, Flow regimes of polymeric fluid droplet formation in a co-flowing microfluidic device, Colloid Interface Sci. Commun. 42 (2021) 100392.
[25] L. Sheng, L. Ma, Y. Chen, J. Deng, G. Luo, A comprehensive study of droplet formation in a capillary embedded step T-junction: from squeezing to jetting, Chem. Eng. J. 427 (2022) 132067.
[26] X. Sun, C. Zhu, T. Fu, Y. Ma, H.Z. Li, Breakup dynamics of elastic droplet and stretching of polymeric filament in a T-junction, Chem. Eng. Sci. 206 (2019) 212–223.
[27] M. Takken, R. Wille, Simulation of pressure-driven and channel-based microfluidics on different abstract levels: a case study, Sensors (2022) 22.
[28] M. Di Martino, D. Ahirwal, P.L. Maffettone, Three-dimensional computational fluid dynamics simulation of the hollow-cone spray process: the stability of the conical liquid sheet, Phys. Fluids 33 (2021).
[29] J.U. Brackbill, D.B. Kothe, C. Zemach, A continuum method for modeling surface tension, J. Comput. Phys. 100 (1992).
[30] T. Glawdel, C. Elbuken, C.L. Ren, Droplet Generation in Microfluidics. Encyclopedia of Microfluidics and Nanofluidics Springer US, 2013, pp. 1–12.
[31] A. Meana-Fernández, J.M. Fernández Oro, K.M. Argüelles Díaz, M. Galdo-Vega, S. Velarde-Suárez, Application of Richardson extrapolation method to the CFD simulation of vertical-Axis wind turbines and analysis of the flow field, Eng. Appl. Comput. Fluid Mech. 13 (2019) 359–376.
[32] P.J. Roache, Quantification of uncertainty in computational fluid dynamics, Annu. Rev. Fluid Mech. 29 (1997).
[33] A. De Masi, P.L. Scognamiglio, E. Battista, P.A. Netti, F. Causa, PEG-based cleavable hydrogel microparticles with controlled porosity for Permiselective trafficking of biomolecular complexes in biosensing applications, J. Mater. Chem. B 10 (2022) 1980–1990.
[34] P. Garstecki, M.J. Fuerstman, H.A. Stone, G.M. Whitesides, Formation of droplets and bubbles in a microfluidic T-junction—scaling and mechanism of break-up, Lab Chip 6 (2006) 437.
[35] M. de Menech, P. Garstecki, F. Jousse, H.A. Stone, Transition from squeezing to dripping in a microfluidic T-shaped junction, J. Fluid Mech. 595 (2008) 141–161.
[36] Y. Pang, Q. Zhou, X. Wang, Y. Lei, Y. Ren, M. Li, J. Wang, Z. Liu, Droplets generation under different flow rates in T-junction microchannel with a neck, AICHE J. 66 (2020).
[37] A. Venkateshwarlu, R.P. Bharti, Effects of capillary number and flow rates on the hydrodynamics of droplet generation in two-phase cross-flow microfluidic systems, J. Taiwan Inst. Chem. Eng. 129 (2021) 64–79.
[38] H. Huynh Thai, P. Silhavy, M. Fajkus, Z. Prokopova, R. Silhavy, Propose-specific information related to prediction level at x and mean magnitude of relative error: a case study of software effort estimation, Mathematics (2022) 10.
[39] A. Gupta, H.B. Eral, T.A. Hatton, P.S. Doyle, Nanoemulsions: formation, properties and applications, Soft Matter 12 (2016) 2826–2841.
[40] G.F. Christopher, S.L. Anna, Microfluidic methods for generating continuous droplet streams, J. Phys. D. Appl. Phys. 40 (2007) R319–R336.
[41] T. Ward, M. Faivre, M. Abkarian, H.A. Stone, Microfluidic flow focusing: drop size and scaling in Pressureversus flow-rate-driven pumping, Electrophoresis 26 (2005) 3716–3724.